Published in final edited form as:
J Nucl Med. 2012 October ; 53(10): 1592–1600. doi:10.2967/jnumed.111.102293.

Immuno-PET imaging of the hepatocyte growth factor receptor Met using the one-armed antibody Onartuzumab (MetMAb)

Elaine M. Jagoda[1,*], **Lixin Lang**[2], **Veerendra Bhadrasetty**[1], **Stephanie Histed**[1], **Mark Williams**[1], **Gabriela Kramer-Marek**[3], **Esther Mena**[1], **Lauren Rosenblum**[1], **Jan Marik**[4], **Jeffrey Tinianow**[4], **Mark Merchant**[4], **Lawrence Szajek**[5], **Chang Paik**[6], **Fabiola Cecchi**[7], **Kristen Raffensperger**[7], **Joe-Marie Jose-Dizon**[7], **Donald P. Bottaro**[7], and **Peter Choyke**[1]

[1]Molecular Imaging Program, National Cancer Institute

[2]Laboratory of Molecular Imaging and Nanomedicine, National Institute of Biomedical Imaging and Bioengineering

[3]Radiation Oncology Branch, National Cancer Institute, National Institutes of Health, Bethesda, MD

[4]Genentech, Inc., South San Francisco, CA

[5]PET, Clinical Center, National Institutes of Health, Bethesda, MD

[6]Nuclear Medicine Departments, Clinical Center, National Institutes of Health, Bethesda, MD

[7]Urologic Oncology Branch, National Cancer Institute, Bethesda, MD

Abstract

The over-expression and -activation of hepatocyte growth factor receptor (Met) in various cancers has been linked to increased proliferation, progression to metastatic disease, and drug resistance. Developing a PET imaging agent to assess Met expression would aid in diagnosis and monitoring responses to Met-targeted therapies. In these studies Onartuzumab (MetMAb), the experimental therapeutic one-armed monoclonal antibody, was radiolabeled with ^{76}Br or ^{89}Zr and evaluated as an imaging agent in Met expressing cell lines and mouse xenografts.

Methods—^{89}Zr-df-Onartuzumab was synthesized using a desferrioxamine-Onartuzumab conjugate (df-Onartuzumab); ^{76}Br-Onartuzumab was labeled directly. Met binding studies were performed using the human tumor-derived cell lines MKN-45, SNU-16 and U87-MG, which have relatively high, moderate and low levels of Met, respectively. Biodistribution and microPET imaging studies were performed in MKN-45 and U87-MG xenografts.

Results—^{76}Br-Onartuzumab and ^{89}Zr-df-Onartuzumab exhibited specific, high affinity Met binding (nM) that was concordant with established Met expression levels. In MKN-45 (gastric carcinoma) xenografts, both tracers cleared slowly from non-target tissues with the highest uptakes in tumor, blood, kidney, and lung. ^{76}Br-Onartuzumab MKN-45 tumor uptakes remained relatively constant from 18 h (5%ID/g) to 48 h (3%ID/g) and exhibited tumor:muscle ratios ranging from 4:1 to 6:1. In contrast, ^{89}Zr-df-Onartuzumab MKN-45 tumor uptake continued to accumulate from 18 h (10%ID/g) to 120 h (23%ID/g), attaining tumor:muscle ratios ranging from 20:1 to 27:1. MKN-45 tumors were easily visualized in imaging studies with both tracers at 18 h but after 48 h ^{89}Zr-df-Onartuzumab image quality improved with at least 2 fold greater tumor uptakes compared to non-target tissues. MKN-45 tumor uptakes for both tracers correlated

[*]Address correspondence: Elaine Jagoda, Molecular Imaging Program/NCI, 10 Center Dr. BLG10/RM B3B69, Bethesda, MD20892-1088, 301-443-1661; 301-480-1434(FAX), ejagoda@mail.nih.gov.

significantly with tumor mass and Met expression, and were not affected by the presence of plasma shed Met.

Conclusions—^{89}Zr-df-Onartuzumab and ^{76}Br-Onartuzumab specifically targeted Met *in vitro* and *in vivo;* ^{89}Zr-df-Onartuzumab achieved higher tumor uptakes and tumor:muscle ratios than ^{76}Br-Onartuzumab at later times suggesting that ^{89}Zr-df-Onartuzumab would be better suited to image Met for diagnostic and prognostic purposes.

Keywords

Immuno-PET imaging; Met receptor; Onartuzumab; MetMAb

The hepatocyte growth factor (HGF) receptor tyrosine kinase (Met) is overexpressed and/or aberrantly activated in a variety of cancers, including gastric, colon, bladder, breast, liver, lungs, pancreatic, esophageal, prostate and cervical carcinomas. (1). Met gene amplification, mutation and/or overexpression in cancer results in increased proliferation, inhibition of apoptosis, tumor angiogenesis and progression to metastatic disease (1, 2). Met amplification or overexpression also has been associated with poor prognosis and drug resistance (3). Together these attributes suggest that the ability to determine changes in Met expression in real time with a Met targeted imaging agent could prove invaluable for diagnosis, patient selection, monitoring disease progression and identifying instances when a Met targeted therapeutic might be beneficial for the patient.

Onartuzumab (MetMAb), a Met selective humanized one-armed monoclonal antibody (~99,000 kDa; derived from IgG1, mAb 5D5), possessing nM affinity for Met has displayed anti-proliferative, anti-angiogenic, and pro-apoptotic properties in mouse tumor models resulting in inhibition of tumor growth (4, 5). Currently Onartuzumab has been studied in Phase I-III clinical trials in which it was well tolerated and NSCLC patients with Met positive tumors showed improved survival (6). The therapeutic effect of Onartuzumab results from competitive antagonism of HGF binding to the Met extracellular domain, thereby preventing pathway activation (5). While high affinity and target specificity of Onartuzumab are desirable attributes required for a PET imaging agent, the slow in vivo clearance of this large protein from the circulation and non-target tissues would require the use of longer lived PET radionuclides thus insuring enough time for clearance of non-target radioactivity but leaving sufficient radioactivity in targeted regions for detection with PET imaging (7, 8). In previous studies by Perk et al (9) the Met specific whole mAb, DN30 (~150 kDa) labeled with the longer lived radionuclide, ^{89}Zr ($t_{1/2}$= 78.4 h) provided semi-quantitative images of human Met expressing tumors in mouse xenografts proving the utility of longer lived radionuclides in compensating for the slow pharmacokinetics of large molecular weight proteins. In addition, the radiolabeled DN30 tumor uptakes corresponded to Met expression levels representing “bivalent” binding to Met and acting as “a partial agonist” resulting in receptor dimerization and phosphorylation. In contrast Onartuzumab is a “pure antagonist” capable of only monovalent binding to the receptor representing quantitatively a 1:1 molar binding ratio{Prat, 1998 #132{Martens, 2006 #62}.

Using the longer lived PET radionuclides, ^{76}Br ($t_{1/2}$= 16.2 h) or ^{89}Zr, we radiolabeled Onartuzumab and evaluated its imaging potential in vitro and in vivo. ^{76}Br was initially selected because it afforded a direct labeling method with little modification of the antibody whereas ^{89}Zr requires a chelate for conjugation to the antibody. The cell lines MKN-45 (human gastric carcinoma), SNU-16 (human gastric carcinoma) and U87-MG (human glioblastoma) which have high, moderate and low Met concentrations, respectively, were used for binding studies to determine the biological activity (% immunoreactivity) and the K_d of ^{76}Br-Onartuzumab and ^{89}Zr-df-Onartuzumab, and in mouse xenograft models to determine the in vivo biodistribution and imaging characteristics of ^{76}Br-Onartuzumab

and ^{89}Zr-df-Onartuzumab (10, 11). Additionally, plasma and tumor samples were collected to evaluate human shed Met ectodomain and tumor Met abundance (Met receptor concentration or density), respectively using immunoassays (10, 12). Met sheds its ectodomain (shed Met), a process in which transmembrane portions of the receptor are proteolytically cleaved and released into the biological circulation. The concentration of shed Met in plasma and urine was found to correlate with tumor burden in mouse xenografts (10). As shed Met may interfere with binding of radiolabeled Onartuzumab, we investigated the relationship between shed Met, tumor Met abundance and tumor mass. Collectively, these studies demonstrate the potential utility of PET labeled Onartuzumab.

Materials and Methods

Cell Lines and Reagents

Cell lines were grown at 37°C and 5% CO_2 in RPMI-1640 (MKN-45 cells), RPMI-1640, 10mM HEPES, 1 mM sodium pyruvate, 4500 mg/L glucose, and 1500mg/L sodium bicarbonate (SNU-16), or DMEM, 0.1 mM NEAA, and 1mM sodium pyruvate (U87-MG). All media were supplemented with 10% FBS, 2mM L-glutamine and Pen/Strep/ Amphotericin B.

Onartuzumab (MetMab) was provided by Genentech, South San Francisco, CA (5). Onartuzumab conjugated to desferrioxamine through an isothiocyanate linker, *p*-Isothiocyanatobenzyl-desferrioxamine-Onartuzumab (df-Onartuzumab) was provided by Jeffrey Tinianow (Genentech, South San Francisco, CA) using a conjugation procedure previously described (13, 14).

Radiosynthesis of ^{76}Br-Onartuzumab and ^{89}Zr-df-Onartuzumab

The radiosynthesis of ^{76}Br-Onartuzumab was accomplished by direct bromination of available tyrosine residues. Briefly, ^{76}Br was produced from ^{75}As (^{3}He, 2n) ^{76}Br reaction and isolated from the solid target by oxidation (15). The radiobrominations were carried out with Onartuzumab (300μgs) in pH6.4 phosphate buffer and aqueous ammonium ^{76}Br-bromide (74-185MBq) in the presence of chloramine-T for 5 min. The product was purified by size exclusion HPLC (Waters Q-TOF MS coupled with a Waters UPLC Acquity system). Typical radiolabeling yield was 45 ± 4.4% (n=10) with a specific activity (EOS) of 0.118 ± 0.067 MBq)/μg (n=10).

The radiosynthesis of ^{89}Zr-df-Onartuzumab was accomplished using a modified method of Perk, et al (13). Briefly, purified ^{89}Zr (IV) in 1 M oxalic acid [74-148MBq] was neutralized with Na_2CO_3 (2M) and HEPES (0.5M, pH7.0) and reacted with df-Onartuzumab (14.7mg/ml, 0.25M $C_2H_3NaO_2$, pH5.5) in ascorbic or gentisic acid (5 mg/mL) and/or 1% BSA for 1 h. Typical labeling yields determined by size exclusion HPLC with UV monitoring were > 90%, with specific activities (EOS) ranging from 0.037-0.185MBq/μg.

In Vitro Studies

Saturation binding studies were done to determine the K_d and B_{max} using plated MKN-45 ($2x10^5$cells/well) and SNU-16 or U87-MG cells in tubes ($2\text{-}10x10^5$cells/tube) to which increasing concentrations of radiolabeled Onartuzumab (0.2-10nM) were added; non-specific binding was determined by adding unlabeled Onartuzumab ($10^{-6.3}$M) to another set of duplicates. Following incubation for 2 h (4°C), the cell bound radiolabeled Onartuzumab was separated from free: 1) plated cells were washed (PBS), treated with trypsin, and collected in vials: 2) cells in tubes were centrifuged and washed twice (PBS); the cell bound radioactivity for these samples was determined by gamma counting (Perkin Elmer2480 Wizard3, Shelton, CT) . The K_d and B_{max} were determined from at least 6 to 8

concentrations of radiolabeled Onartuzumab and analyzed using non-linear regression curve fits (one-site binding hyperbola) [PRISM (version3.02Windows), Graphpad software, San Diego, CA].

One of two methods was used to determine the immunoreactive fractions or biological specific activity of the radiolabeled Onartuzumab as previously described (16). Briefly, a modified method described by Lindmo et al. (17) was used in which the immunoreactivity was calculated by extrapolation to infinite antigen excess conditions. Alternatively, a modification of the specific activity determination by self-displacement technique described by Morris (18) which is derived from a radiolabeled Onartuzumab saturation curve and competition curve with unlabeled Onartuzumab.

Mouse Tumor Models

Athymic female nude mice (Ncr-nu/nu, NCI-Frederick, MD) were injected subcutaneously in the right thigh with MKN-45 or U87-MG cells (5- $8x10^6$) in PBS:30% matrigel. All animal studies were performed in accordance with NIH Guidelines for the Care and Use of Laboratory Animals using IACUC approved protocols.

Biodistribution Studies

Nude or tumor (50-1000 mg)-bearing mice were injected awake intravenously (tail vein) with either ^{76}Br-Onartuzumab [0.185-0.74MBq(2-5 μg)], ^{89}Zr-df-Onartuzumab [0.37-1.85MBq(3-46 μg)], ^{89}Zr-oxalate (neutralized) [0.185-0.74MBq] and euthanized (CO_2 inhalation) at selected times. Blood (cardiac puncture) and tissues were excised from each animal, weighed, and the radioactive concentration determined (Perkin Elmer2480 Wizard3). The radioactivity in the blood and each tissue was expressed as %Injected dose per gram of tissue (%ID/g) normalized to a 20g mouse: $100 \times [(cpm_{tissue})/(cpm_{injected\ dose}) \times (\text{tissue weight (g)})] \times [(\text{body weight})/(20)]$. Immediately following counting, tumor samples were fast frozen and stored at -70°C for determination of Met content. An additional blood sample was collected in EDTA coated tubes and after centrifugation the separated plasma samples were fast frozen and stored at -70°C for shed Met analysis.

For the blocking studies with unlabeled Onartuzumab, MKN-45 tumor (50-200 mg) -bearing mice were divided into 2 groups with one group receiving ^{89}Zr-df-Onartuzumab [∼0.37MBq(∼ 3 μg)] and the other group receiving a coinjection of ^{89}Zr-df-Onartuzumab +1 mg unlabeled Onartuzumab. The mice were euthanized after 3 days and the processing of the blood and tissues was performed as described above. Statistical analysis of the differences between the 2 groups was done using the student t test.

MicroPet Imaging Studies

Tumor-bearing mice were anesthetized using isoflurane/O_2 (1.5%-3% v/v) and imaged at various times after intravenous injection of ^{76}Br- Onartuzumab [1.85-5.55MBq (30-50μg)] or ^{89}Zr-df-Onartuzumab [3.7-7.4MBq (64-128μg)]. Whole body static images were obtained requiring 4-5 bed positions (FOV= 2.0 cm, total imaging time:20-25 min) using the Advanced Technology Laboratory Animal Scanner (ATLAS) (19) . The images were reconstructed by a two dimensional ordered-subsets expectation maximum from which region of interests (ROIs) were drawn manually to determine the tissue uptakes (kBq/cc). The %ID/g normalized to a 20g mouse was then determined using the formula: $[(100 \times (\text{tissue uptake})/(\text{Injected Dose})] \times [(\text{body weight})/(20)]$.

Determination of plasma shed Met ectodomain and total tumor Met

Met and plasma Met ectodomain (shed Met) levels were measured using a two-site electrochemiluminescent immunoassay in which antibodies tagged with a ruthenium chelate (MSD Sulfo-Tag) are detected with a Meso Scale Discovery (MSD) SectorImager 2400 plate reader as described previously (10). Purified recombinant Met ectodomain–Ig fusion protein was used as a reference standard for quantitation of Met mass per mass total extracted cell protein. Tumor tissue extracts were prepared by physically disrupting tissue samples before clearing by centrifugation, and analysis of Met content as described above. Correlations of shed Met, total tumor Met, tumor radioactive Onartuzumab content to tumor mass or total tumor mass were performed using the Spearman rank correlation coefficient (PRISM (version3.02Windows), Graphpad software, San Diego, CA)

Results

In Vitro Cell Binding Studies

Binding studies were performed with ^{76}Br-Onartuzumab and ^{89}Zr--df-Onartuzumab to determine the, affinity (K_d), concentration of Met (B_{max}, receptors per cell), and the % immunoreactive fraction using MKN-45 cells (11). Both ^{76}Br-Onartuzumab and ^{89}Zr-df-Onartuzumab had high specific binding for Met ranging from 80-96% and 80-98%, respectively. The K_d for ^{76}Br-Onartuzumab binding was 5.14 ± 0.81 nM (n=3), which was comparable to the K_d for ^{89}Zr-df-Onartuzumab binding, 6.12 ± 1.18 nM (n=3). The estimated numbers of receptors per cell (calculated from B_{max}) were 1.07 ± 0.28 x10^6 (n=3) and 0.936 ± 0.08 x10^6 (n=3) for ^{76}Br-Onartuzumab and ^{89}Zr-df-Onartuzumab, respectively. The % immunoreactive fractions were also comparable, 85.4 ± 6.9 % (n=3) and 81.9 ± 0.7 % (n=3) for ^{76}Br-Onartuzumab and ^{89}Zr-df-Onartuzumab, respectively. In similar saturation studies with SNU-16 and U87-MG, higher non-specific binding was observed ranging from 20-30% and 55-85%, respectively, which is consistent with moderate and lower levels of Met expression (10, 11). The B_{max} for SNU-16 [0.089 ± 0.013 × 10^6 (n=3)] was at least 6 fold higher than for U87-MG [0.014 ± 0.003 × 10^6 (n=3)]. These data compare favorably with the expected levels of Met expression for these human cancer cell lines and further indicate that these tracers would be appropriate for imaging tumors with high to moderate Met expression (>100,000 receptors per cell) but at lower Met expression levels (< 14,000 receptors per cell), non-specific interactions could impair the detection of specific Met binding.

In Vivo ^{76}Br-Onartuzumab, ^{89}Zr-df-Onartuzumab, and ^{89}Zr-oxlate Biodistribution Studies

The biodistribution of ^{76}Br-Onartuzumab was determined in MKN-45 xenografts from 6 to 72 h (Fig. 1A). The highest uptakes were observed in tumor, blood, kidney, and lung with tumor uptakes similar to the blood and these non-target organs at all time points. In similar biodistribution studies using U87-MG xenografts, uptakes in non-target tissues were comparable to MKN-45 xenografts but tumor uptakes were ∼2 fold lower, consistent with its lower Met content. Examining the ratio of %ID/g in the tumor and muscle (a non-target tissue) to further assess feasibility as an imaging agent, revealed that the highest tumor:muscle ratios (T:M), 5:1 to 6:1, occurred after 24 h for MKN-45 xenografts (Table 1). For the U87 xenografts, the T:M ratio ranged from 3:1 to 4:1 at 24 and 48 h, or ∼1.5-2 fold lower, consistent with lower Met expression.

Since uptakes of ^{76}Br-Onartuzumab in blood and tumors were similar over time, studies were undertaken to determine if the levels of shed Met ectodomain in the blood of tumor-bearing mice differed from those of control mice, potentially influencing the blood clearance. Both of these Met expressing tumors have been shown to shed Met ectodomain into the systemic circulation (10, 11). For these studies, the biodistribution of ^{76}Br-

Onartuzumab was determined in non-tumor bearing nude mice after 6, 16, 24 and 48 h and compared to the uptakes (%ID/g) shown in Fig.1A (MKN-45 xenografts). At all time points, the %ID/g in blood (Fig. 1B), heart, kidneys, lungs, or spleen were not significantly different ($P < 0.05$); significant differences were observed in liver uptakes at 6 h (28% decrease) and in muscle at 6 h (24% decrease), 16 h (47% decrease), and 48 h (53% increase) in the nude mice vs the xenografts. The differences in muscle uptake may be attributable to poor counting statistics since this tissue has relatively low radioactivity. The significant difference in the liver uptakes most likely reflects age and body weight differences between the 2 groups. Although the uptakes were normalized to a 20g mice this does not take into account age related changes in metabolism which in this case the xenograft mice at 6 h were older mice (∼12 weeks) weighing almost 30g compared to the nude mice which were younger (∼5 weeks) weighing between 19-24g, hence the younger nude mice would be expected to have faster liver metabolism and clearance compared to the older xenograft mice resulting in the observed decreased liver uptakes. Further the concentration of shed Met ectodomain (Fig.1B; ng/mL per g of tumor mass) in plasma samples obtained from these MKN-45 xenografts remained relatively unchanged at 16, 24, and 48 h whereas the ^{76}Br-Onartuzumab blood uptakes were steadily decreasing. The ^{76}Br-Onartuzumab blood concentration (at time of injection) was ∼12 nM which was ∼100 fold excess compared to shed Met blood concentrations of ∼ 0.126 nM for a 1g tumor (representative of the largest tumor and highest shed Met blood concentration). Overall these results indicate that the presence of shed Met in tumor-bearing mice does not alter the pharmacokinetics and clearance of ^{76}Br-Onartuzumab.

The biodistribution of ^{89}Zr-df-Onartuzumab was determined in MKN-45 xenografts from 18 h to 5 d (Fig 2). ^{89}Zr-df-Onartuzumab uptakes (%ID/g) in the non-target tissues, blood, heart, lungs, gastrointestinal tract (GI) and muscle, decreased slowly with less than a 50% reduction in %ID/g from 18 h to 5 d. In contrast, uptakes in the liver and kidney increased over the time course, suggestive of hepatobiliary and renal clearance. At 18 h ^{89}Zr-df-Onartuzumab tumor uptakes were comparable to that of blood, kidney and lung, but from 2-5 days tumor uptakes were at least 2 fold greater than that of blood, kidney and lung. At 2, 3, 4 and 5 days the tumors had the highest uptakes, ranging from 16.5-22.5%ID/g. In a similar biodistribution study using U87-MG xenografts, the uptake in non-target tissues was comparable to the results of the MKN-45 xenograft study shown in Fig. 2. However, uptake in the U87 tumor was 1.8 and 3.0 fold lower than the MKN-45 tumors at 3 and 5 days, respectively. The highest tumor:muscle ratios (T:M) of 13.2, 26.5 and 26.6, occurred at 2, 3 and 5 days, respectively, for the MKN-45 xenografts, while T:M for the U87 xenografts ranged from 7:1 to 9:1 over the 5 day time course (Fig 3). The 2-3 fold reduction in uptake by U87 tumors is consistent with the lower Met expression of this cell line

Blocking studies were performed with MKN-45 xenografts in which ^{89}Zr-df-Onartuzumab (0.0133 nmoles Onartuzumab), or ^{89}Zr-df-Onartuzumab + 10 nmoles of unlabeled Onartuzumab, were injected. Uptakes (%ID/g) determined after 3 d were comparable for both groups in blood, heart, lungs, spleen, liver, GI, and muscle. Kidney uptake increased ∼ 2.5 fold and tumor uptake decreased ∼ 3.8 fold, suggesting competitive blocking by unlabeled Onartuzumab in the tumor. The T:M ratios for the blocked group were significantly reduced (67%, $P< 0.05$) compared to mice injected with ^{89}Zr-df-Onartuzumab alone, indicating specific Met binding *in vivo* (Fig. 3).

To determine the biological fate of free ^{89}Zr that may result from ^{89}Zr-df-Onartuzumab metabolism, the biodistribution of ^{89}Zr-oxalate (which has a biodistribution characteristic of Zr (20)) was determined in MKN-45 xenograft mice from 1 to 5 d (Fig.4). The highest retention and accumulation of radioactivity ranging from 20 to 30%ID/g occurred in bone over the entire course and was 3 to 8 fold higher than ^{89}Zr-df-Onartuzumab bone uptakes.

The greatest clearance of radioactivity from 1 to 5 d was observed in the blood (> 90%), while clearance from other tissues was slower (55% to 10% decreases). The tumors retained at least 80% of the radioactivity from 1 to 5 d with uptakes ranging from 2.1-2.6%ID/g which were higher than all other tissues except bone. ^{89}Zr tumor uptakes (2%ID/g) represented <10% of ^{89}Zr-df-Onartuzumab tumor uptakes of 22% and 25% at 3 and 5 d, respectively.

The uptakes (%ID/g) of ^{89}Zr-df-Onartuzumab and ^{76}Br-Onartuzumab, in blood, muscle and MKN-45 tumors from 6 to 120 h are compared in Fig. 5. ^{89}Zr-df- Onartuzumab tumor uptakes remained steady or increased over the 5 day time course whereas ^{76}Br-Onartuzumab tumor uptakes steadily decreased over the 3 d time course (Fig. 5). Although muscle uptake over time was similar for both tracers, the radioactivity remaining in the blood of each agent differed. After 2 d ^{89}Zr-df-Onartuzumab tumor uptake exceeded the blood levels, whereas ^{76}Br- Onartuzumab tumor uptake mirrored blood levels over the entire time course. Thus ^{76}Br-Onartuzumab showed lower retention in the tumors relative to ^{89}Zr-df-Onartuzumab with clearance similar to the radioactivity in blood.

^{89}Zr-df-Onartuzumab had the highest tumor: muscle ratios (T:M) of 19.6 and 26.6 at 96 and 120 h, respectively (Table 1). Over the entire time course of the ^{76}Br-Onartuzumab, the T:M were ∼ 2 fold lower than the ^{89}Zr-df-Onartuzumab T:M (Table 1). The ^{76}Br-Onartuzumab T:M remained relatively unchanged from 24 to 72 h, whereas ^{89}Zr-df-Onartuzumab T:M increased from 24 to 120 h (Table 1). Similarly, ^{76}Br-Onartuzumab tumor to blood ratios were always < 1 at 6, 16, 24, 48, and 72 h, while ^{89}Zr-df-Onartuzumab T:M ratios were ∼2 at 72 h and increased to ∼4 at 120 h.

MicroPET Imaging Studies

MicroPET imaging studies with ^{76}Br-Onartuzumab were performed in MKN-45 or U87-MG xenografts with imaging from 18 h to 3 d. MKN-45 tumors were visualized as early as 18 h with image quality improving at 24 h, attaining a T:M ratio of ∼ 5 (Fig. 6A). Despite increasing the ^{76}Br-Onartuzumab dose from 11.1 to 18.5 MBq, images obtained at 48 h and 72 h showed no improvement, due to relatively low levels of radioactivity and lack of ^{76}Br-Onartuzumab retention in tumors; therefore 24 h proved to be the optimum imaging time. In U87-MG xenografts at 24 h, tumors were more difficult to discern compared to the MKN-45 tumors, consistent with their lower Met expression level.

Imaging studies of MKN-45 xenografts with ^{89}Zr-df-Onartuzumab indicated that although tumors could be visualized at 18 h, image quality improved over the 5 day period (Fig. 6B). At 5 days the MKN-45 T:M ratio was 26:1; the increase in T:M ratios over the 5 day period reflects better tumor retention and clearance from non-target tissues.

Correlation of ^{76}Br-Onartuzumab and ^{89}Zr-df-Onartuzumab uptakes with shed Met and tumor Met

Plasma and tumor samples from naïve MKN-45 xenografts or MKN-45 xenografts injected with ^{76}Br-Onartuzumab or ^{89}Zr-df-Onartuzumab were analyzed for shed Met ectodomain and total tumor Met content and then the potential associations between these values to tumor mass and/or the total tumor radioactive content [% Injected dose (%ID) per tumor] were determined (Fig.7A-F). In naïve xenografts, significant direct correlations were found between tumor mass and shed Met (Fig.7A), tumor mass and total tumor Met content (Fig. 7B), and total tumor Met content and shed Met (Fig.7C). The total Met contents of tumor samples excised from ^{89}Zr-df-Onartuzumab injected xenografts were also significantly correlated with the tumor mass (Fig.7E) and with the ^{89}Zr-df-Onartuzumab total tumor uptakes (%ID) (Fig.7F); similar results were obtained using tumor samples from ^{76}Br-

Onartuzumab injected xenografts (data not shown). The similarity in correlations from naïve tumors vs ^{76}Br-Onartuzumab or ^{89}Zr-df-Onartuzumab -labeled tumors indicates that the tracer did not interfere with the Met content determinations. The lower slope observed in the correlation of ^{76}Br-Onartuzumab tumor uptakes to tumor mass compared to that of ^{89}Zr-df-Onartuzumab (Fig.7D) most likely reflects the overall decreased tumor retention of ^{76}Br-Onartuzumab. The significant correlations between ^{89}Zr-df-Onartuzumab or ^{76}Br-Onartuzumab tumor uptakes) and total tumor Met content (Fig.7F) indicate that radiolabeled Onartuzumab tumor uptakes directly reflect tumor Met concentrations. Plasma shed Met values from ^{76}Br-Onartuzumab or ^{89}Zr-df-Onartuzumab injected xenografts also correlated significantly with tumor mass (data not shown; $P < 0.0001$ and < 0.03, respectively), comparable to results with the naïve xenografts, indicating that neither ^{76}Br-Onartuzumab nor ^{89}Zr-df-Onartuzumab affected Met shedding.

Discussion

Onartuzumab labeled with ^{76}Br or ^{89}Zr retained the majority of its biological activity (> 80% immunoreactivity) and displayed nanomolar binding affinity for Met. Both agents could quantitatively distinguish a high Met expressing cell line (MKN-45) from a low Met expressing cell line (U87-MG) *in vitro*. Although these *in vitro* parameters were similar, *in vivo* biodistribution and imaging studies revealed that ^{89}Zr-df-Onartuzumab attained higher tumor to non-target tissue ratios over time providing higher quality images than ^{76}Br-Onartuzumab in MKN-45 xenografts.

^{76}Br-Onartuzumab did not accumulate in MKN-45 tumors at later time points but decreased at a rate similar to non-target tissues, resulting in no improvement of T:M ratios over time compared to ^{89}Zr-df-Onartuzumab. The lack of further accumulation may in part, be related to the direct labeling method used for ^{76}Br-Onartuzumab; available tyrosine residues are labeled in the presence of a strong oxidizing agent, and excessive protein oxidation can result in lower immunoreactivity. In addition, directly labeled antibodies internalized into cells are characteristically subject to debromination, thereby losing their label (21). Although in this case, Onartuzumab behaves as an antagonist, unable to cause dimerization, internalization would expected to be minimal and not necessarily mediated by activation of Met (22). Since ^{76}Br-Onartuzumab immunoreactivity was preserved in our studies, *in vivo* debromination and metabolism are most likely responsible for the lower tumor uptakes relative to ^{89}Zr-df-Onartuzumab. Alternative radiosynthetic methods have been described for labeling antibodies with ^{76}Br, including indirect methods and an enzymatic method (bromoperoxidase) which claim to improve *in vivo* stability and thereby increase tumor accumulation and retention (7).

In contrast, indirectly labeled metal-chelate coupled antibodies like ^{89}Zr-df-Onartuzumab tend to have increased accumulations in target cells due to trapping of radioactive metabolites from internalization(21). Our results are similar to other studies in which tumor uptakes were increased with MAbs labeled with ^{89}Zr, a “residualizing” radionuclide compared to ^{124}I, a non-residualizing radionuclide (9). We observed substantially greater retention of ^{89}Zr-df-Onartuzumab in MKN-45 tumors (22 and 25 % ID/g at 3 and 5 d, respectively) compared to the tumor retention of ^{89}Zr-oxalate (2.1 and 2.2%ID/g at 3 and 5 d, respectively) indicating that the majority of the tumor uptake would be expected to represent binding to Met rather than free ^{89}Zr.

Although ^{89}Zr-df-Onartuzumab uses an indirect labelling method conferring increased tumor retention, we observed high bone uptakes ranging between 6 and 7%ID/g at 3 and 5 d, respectively, which could theoretically impact clinical application. In agreement with our results, ^{89}Zr-oxalate and other solvated or chelated forms of ^{89}Zr had high bone

accumulations in mice which was primarily associated with the bone and epiphyses rather than bone marrow(20). Further Abou, et al. showed that the bone uptake was dependent on the strength of the chelate. While these pre-clinical mouse studies would predict potentially high bone uptakes of free ^{89}Zr in human studies, successful ^{89}Zr immuno-PET clinical studies have been done in which bone uptakes and radiation doses to bone marrow were minimal (23). These studies would suggest that with the appropriate radiochemistry and a strong chelate, that high ^{89}Zr bone uptakes can be avoided.

In addition to the longer radioactive half-life which better accommodates the longer biological half-life of Onartuzumab and increased tumor retention, ^{89}Zr-df-Onartuzumab in vivo tumor uptakes were Met specific and sensitive to changes in Met densities. Unlabeled Onartuzumab significantly blocked tumor uptakes indicating that ^{89}Zr-df-Onartuzumab and Onartuzumab are competing for the same binding site. The substantially decreased ^{89}Zr-df-Onartuzumab uptakes observed in U87-MG tumors relative to MKN-45 tumors represents reduced Met densities in U87-MG tumors which are known to have low Met expression. Further the significant correlations between ^{89}Zr-df-Onartuzumab tumor uptake, tumor mass and total tumor Met content confirm that ^{89}Zr-df-Onartuzumab tumor uptake is directly related to tumor Met density. However, in larger tumors ^{89}Zr-df-Onartuzumab uptakes maybe decreased due to necrosis rather than real changes in Met densities of the viable tumor tissue. In this case for the ^{89}Zr-df-Onartuzumab uptake to accurately correspond to the tumor Met density, “viable uptakes” excluding the necrotic regions would need to be determined from the PET images. The presence of shed Met did not appear to alter the ^{76}Br-Onartuzumab biodistributions in nude mice vs MKN-45 xenografts which is most likely a consequence of the high molar ratio of ^{89}Zr-df-Onartuzumab to shed Met (>100 fold). Although shed Met concentrations were comparable from naïve and radiolabeled Onartuzumab which would suggest radiolabeled Onartuzumab does not interact with shed Met, this does not preclude the possibility that radiolabeled Onartuzumab binds to a distinct site that does not crossreact with the immunoassay detection antibody. More importantly these results indicate that shed Met would not be expected to interfere with delivery of radiolabeled Onartuzumab to its target.

These results indicate that ^{89}Zr-df-Onartuzumab may prove to be an effective immuno-PET imaging agent in humans. It is important to note, however, that Onartuzumab does not recognize murine Met, and thus our preclinical studies do not address Onartuzumab uptake that might occur in human tissues that normally express Met. Initial imaging studies in humans with ^{89}Zr-df-Onartuzumab designed to determine uptake in non-target tissues will be important for determining imaging feasibility. Since ^{89}Zr-df-Onartuzumab represents the radiolabeled version of the therapeutic Onartuzumab, this agent may aid in drug development by identifying tissues that may be subject to Onartuzumab-associated toxicities, assessing responses to Onartuzumab treatment, establishing appropriate dosing for optimal tumor targeting, and tracking in vivo the disposition of Onartuzumab in individual patients. ^{89}Zr-df-Onartuzumab imaging may also prove useful in the development of small molecule Met TKIs and other Met targeted agents for monitoring therapeutic responses in which decreased uptakes would be expected in Met positive tumors. More generally, ^{89}Zr-df-Onartuzumab has potential utility for imaging Met to identify patients for treatment with Met-targeted therapeutics and to identify the emergence of Met-driven acquired resistance to other molecularly targeted cancer therapies.

References

1. Birchmeier C, Birchmeier W, Gherardi E, Vande Woude GF. Met, metastasis, motility and more. Nature reviews. 2003; 4:915–925.

2. Peruzzi B, Bottaro DP. Targeting the c-Met signaling pathway in cancer. Clin Cancer Res. 2006; 12:3657–3660. [PubMed: 16778093]
3. Cappuzzo F, Janne PA, Skokan M, et al. MET increased gene copy number and primary resistance to gefitinib therapy in non-small-cell lung cancer patients. Ann Oncol. 2009; 20:298–304. [PubMed: 18836087]
4. Jin H, Yang R, Zheng Z, et al. MetMAb, the one-armed 5D5 anti-c-Met antibody, inhibits orthotopic pancreatic tumor growth and improves survival. Cancer research. 2008; 68:4360–4368. [PubMed: 18519697]
5. Martens T, Schmidt NO, Eckerich C, et al. A novel one-armed anti-c-Met antibody inhibits glioblastoma growth in vivo. Clin Cancer Res. 2006; 12:6144–6152. [PubMed: 17062691]
6. Surati M, Patel P, Peterson A, Salgia R. Role of MetMAb (OA-5D5) in c-MET active lung malignancies. Expert Opin Biol Ther. 2011; 11:1655–1662. [PubMed: 22047509]
7. Nayak TK, Brechbiel MW. Radioimmunoimaging with longer-lived positron-emitting radionuclides: potentials and challenges. Bioconjug Chem. 2009; 20:825–841. [PubMed: 19125647]
8. Verel I, Visser GW, Boellaard R, et al. Quantitative 89Zr immuno-PET for in vivo scouting of 90Y-labeled monoclonal antibodies in xenograft-bearing nude mice. J Nucl Med. 2003; 44:1663–1670. [PubMed: 14530484]
9. Perk LR, Stigter-van Walsum M, Visser GW, et al. Quantitative PET imaging of Met-expressing human cancer xenografts with 89Zr-labelled monoclonal antibody DN30. European journal of nuclear medicine and molecular imaging. 2008; 35:1857–1867. [PubMed: 18491091]
10. Athauda G, Giubellino A, Coleman JA, et al. c-Met ectodomain shedding rate correlates with malignant potential. Clin Cancer Res. 2006; 12:4154–4162. [PubMed: 16857786]
11. Bachleitner-Hofmann T, Sun MY, Chen CT, et al. HER kinase activation confers resistance to MET tyrosine kinase inhibition in MET oncogene-addicted gastric cancer cells. Mol Cancer Ther. 2008; 7:3499–3508. [PubMed: 18974395]
12. Martin TA, Jiang WG. Hepatocyte growth factor and its receptor signalling complex as targets in cancer therapy. Anticancer Agents Med Chem. 2010; 10:2–6. [PubMed: 20015008]
13. Perk LR, Vosjan MJ, Visser GW, et al. p-Isothiocyanatobenzyl-desferrioxamine: a new bifunctional chelate for facile radiolabeling of monoclonal antibodies with zirconium-89 for immuno-PET imaging. European journal of nuclear medicine and molecular imaging. 2009; 37:250–259. [PubMed: 19763566]
14. Verel I, Visser GW, Boellaard R, Stigter-van Walsum M, Snow GB, van Dongen GA. 89Zr immuno-PET: comprehensive procedures for the production of 89Zr-labeled monoclonal antibodies. J Nucl Med. 2003; 44:1271–1281. [PubMed: 12902418]
15. Szajek LP, Kao CH, Kiesewetter DO, et al. Radiochimica Acta. 2004; 92:291–295.
16. Choi CW, Lang L, Lee JT, et al. Biodistribution of 18F- and 125I-labeled anti-Tac disulfide-stabilized Fv fragments in nude mice with interleukin 2 alpha receptor-positive tumor xenografts. Cancer research. 1995; 55:5323–5329. [PubMed: 7585595]
17. Lindmo T, Boven E, Cuttitta F, Fedorko J, Bunn PA Jr. Determination of the immunoreactive fraction of radiolabeled monoclonal antibodies by linear extrapolation to binding at infinite antigen excess. J Immunol Methods. 1984; 72:77–89. [PubMed: 6086763]
18. Morris BJ. Specific radioactivity of radioimmunoassay tracer determined by self-displacement: a re-evaluation. Clin Chim Acta. 1976; 73:213–216. [PubMed: 1000834]
19. Seidel J. Resolution uniformity and sensitivity of the NIH atlas small animal scanner: comparison to simulated LSO scanners without depth-of-interaction capability. IEEE Trans Nucl Sci. 2003; 50:1347–1357.
20. Abou DS, Ku T, Smith-Jones PM. In vivo biodistribution and accumulation of 89Zr in mice. Nucl Med Biol. 2011; 38:675–681. [PubMed: 21718943]
21. Wu AM, Olafsen T. Antibodies for molecular imaging of cancer. Cancer journal (Sudbury, Mass. 2008; 14:191–197.
22. Prat M, Crepaldi T, Pennacchietti S, Bussolino F, Comoglio PM. Agonistic monoclonal antibodies against the Met receptor dissect the biological responses to HGF. J Cell Sci. 1998; 111(Pt 2):237–247. [PubMed: 9405310]

23. Borjesson PK, Jauw YW, de Bree R, et al. Radiation dosimetry of 89Zr-labeled chimeric monoclonal antibody U36 as used for immuno-PET in head and neck cancer patients. J Nucl Med. 2009; 50:1828–1836. [PubMed: 19837762]

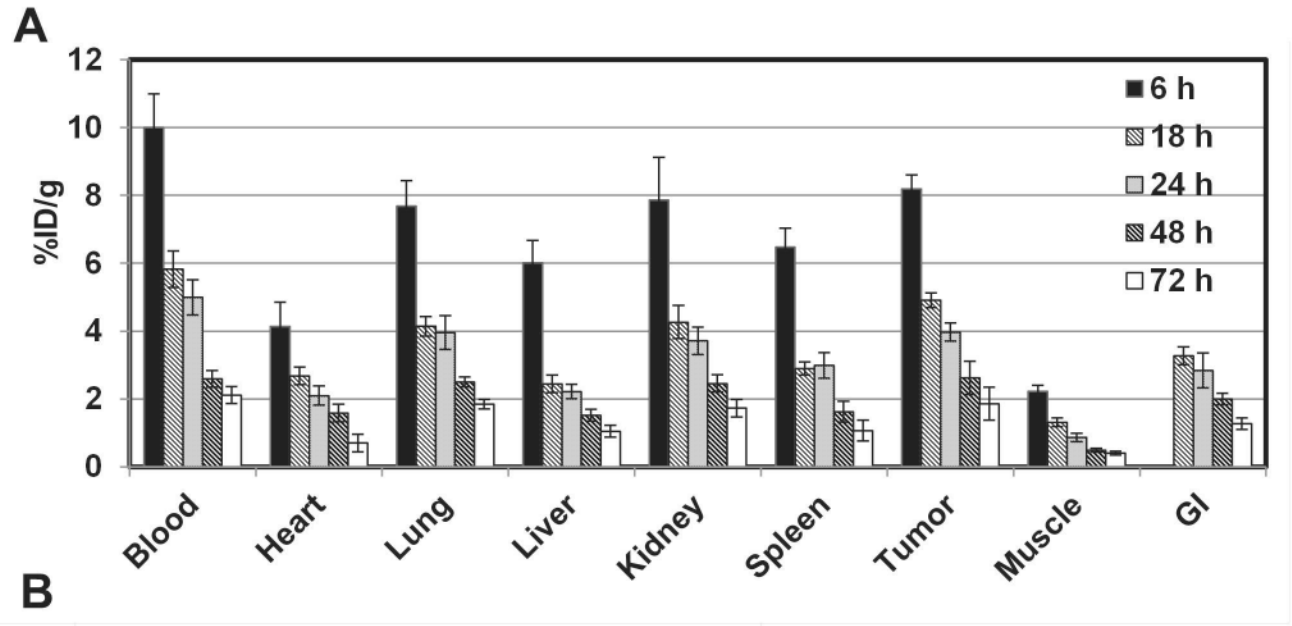

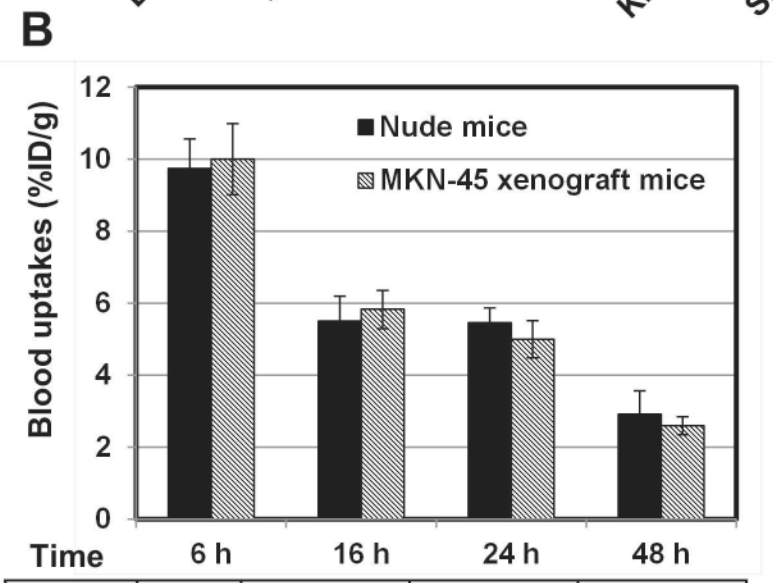

Shed Met (ng/mL /g tumor)	ND	12.9 ± 4.4	12.7 ± 3.6	14.1 ± 5.2

FIGURE 1.

A) Biodistribution of ^{76}Br-Onartuzumab in MKN-45 xenografts *from 6 to 72 h*. Each time point represents the mean %ID/g ± SD of ^{76}Br-Onartuzumab (n=3 for 72 h group; n=4 for all other time points). **B)** Comparison of ^{76}Br-Onartuzumab blood uptakes (%ID/g) in nude and MKN-45 xenograft mice. Each time point represents the mean %ID/g ± SD of ^{76}Br-Onartuzumab (nude mice, n=5; MKN-45 xenografts, n=4). The table below are the corresponding plasma shed Met ectodomain concentrations (ng/mL/g tumor) determined from the same MKN-45 xenograft mice blood samples; each value represents the mean concentration ± SD (n=4; ND-not determined).

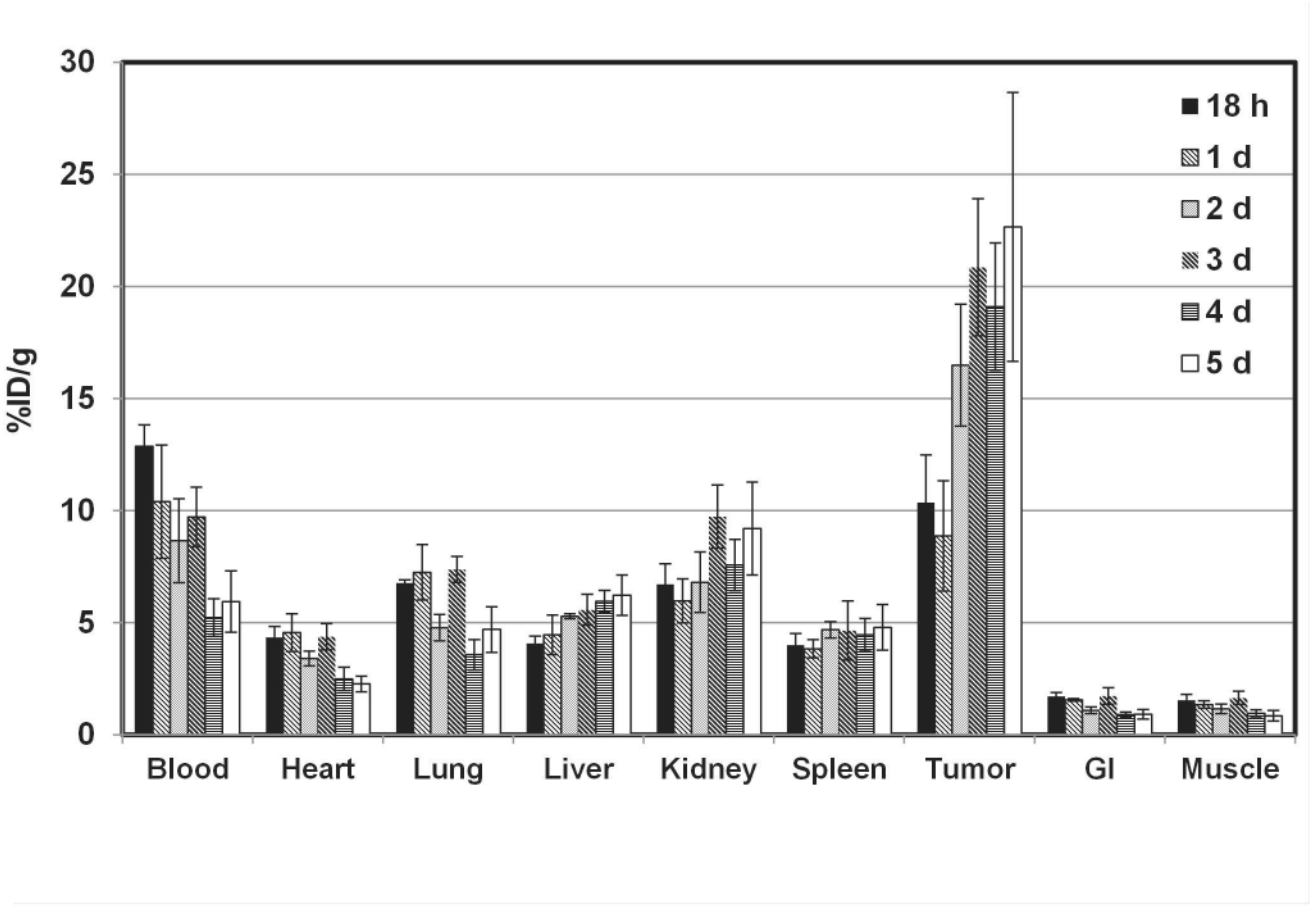

FIGURE 2.

Biodistribution of ^{89}Zr-df-Onartuzumab in MKN-45 xenografts *from 18 h to 5 d*. Each bar represents %ID/g ± SD of ^{89}Zr-df-Onartuzumab (n=5, 18 h group; n=4, other time points).

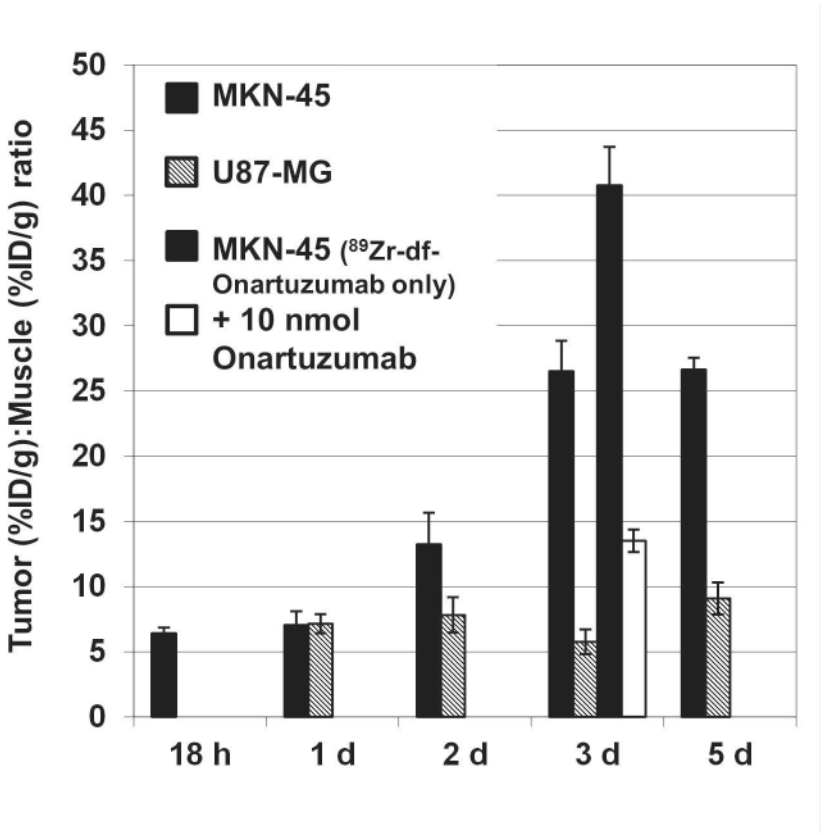

FIGURE 3.

Comparison of Tumor (%ID/g):Muscle (%ID/g) Ratios (T:M) of ^{89}Zr-df-Onartuzumab in MKN-45 and U87-MG xenografts *from 18 h to 5 d*. Bars represent mean T:M ± SD (n= 4). Bars at 3 d include T:M from ^{89}Zr-df-Onartuzumab competitive blocking study in MKN-45 xenografts injected with ^{89}Zr-df-Onartuzumab only or ^{89}Zr-df-Onartuzumab + 10 nmoles Onartuzumab.

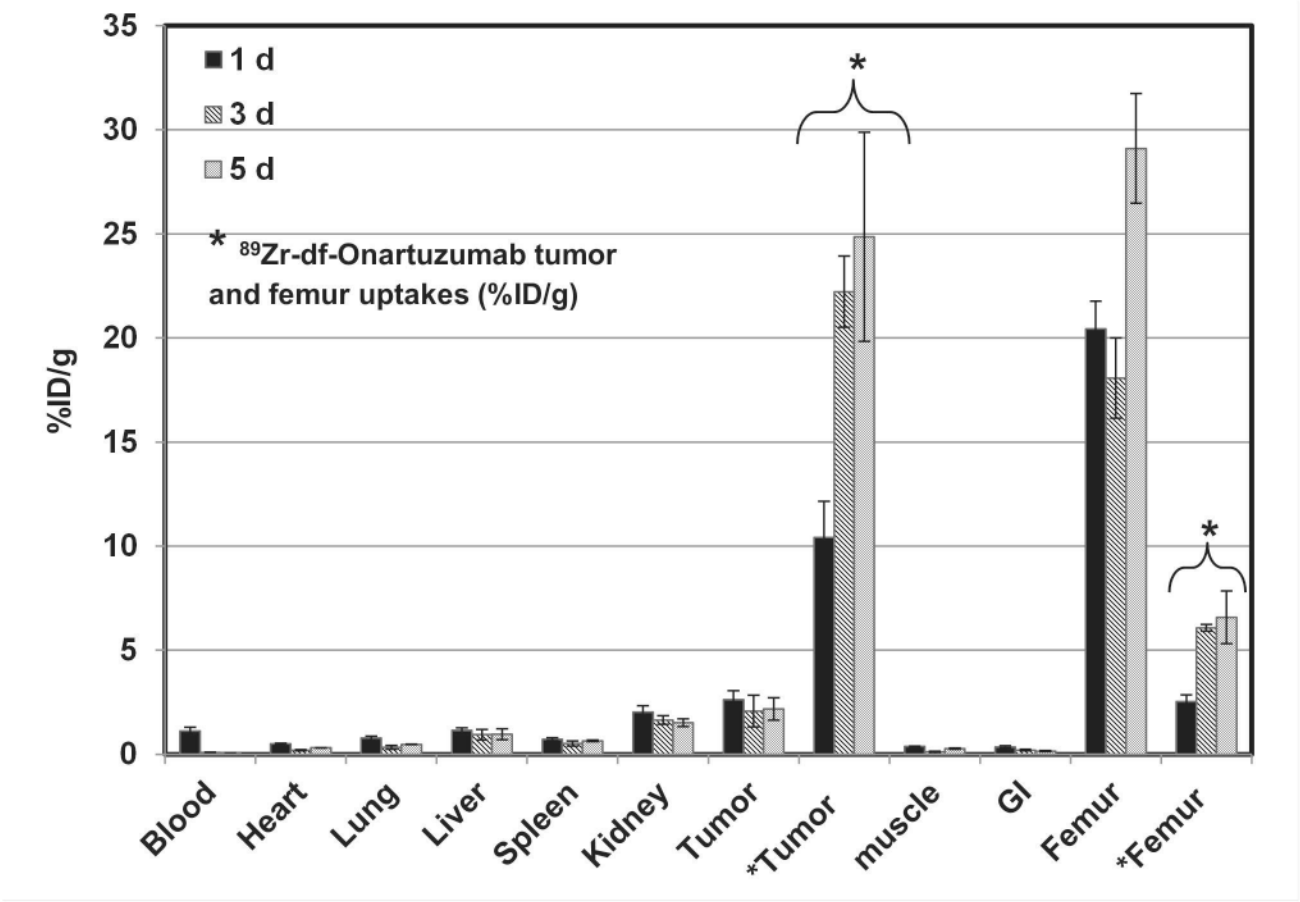

FIGURE 4.

Biodistribution of ^{89}Zr-oxalate in MKN-45 xenografts after 1, 3, and 5 d and for comparison ^{89}Zr-df-Onartuzumab tumor and femur uptakes (*, %ID/g). Each bar represents %ID/g ± SD ([^{89}Zr]-oxalate, n=3; ^{89}Zr-df-Onartuzumab, n= 3).

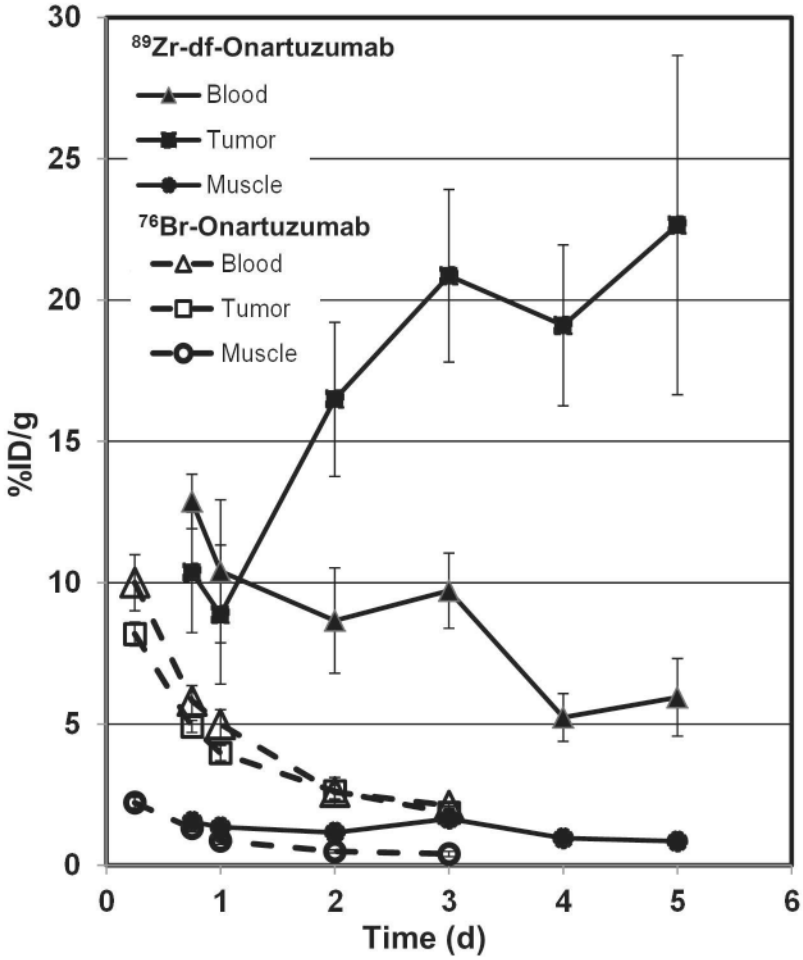

FIGURE 5.

Comparison of the blood, tumor and muscle uptakes of ^{89}Zr-df-Onartuzumab and ^{76}Br-Onartuzumab in MKN-45 xenografts from 6 h to 5 d. Each bar represents %ID/g ± SD of ^{89}Zr-df-Onartuzumab [(n= 5 (18 h); n=4 (other times) or [^{76}Br]Onartuzumab (n= 4)].

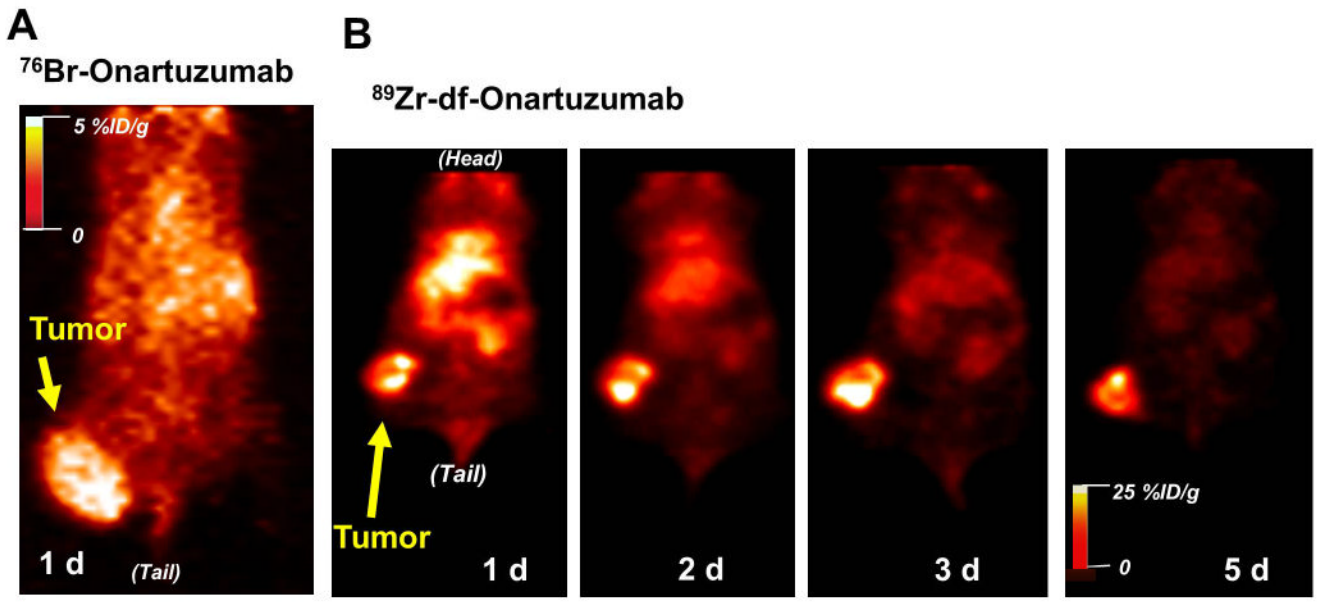

FIGURE 6.

Representative coronal PET images from a mouse with a MKN-45 tumor on the right thigh injected with: **A)** ^{76}Br-Onartuzumab (tumor volume ~ 0.7 cc); **B**) ^{89}Zr-df-Onartuzumab (tumor volume ~ 0.4 cc).

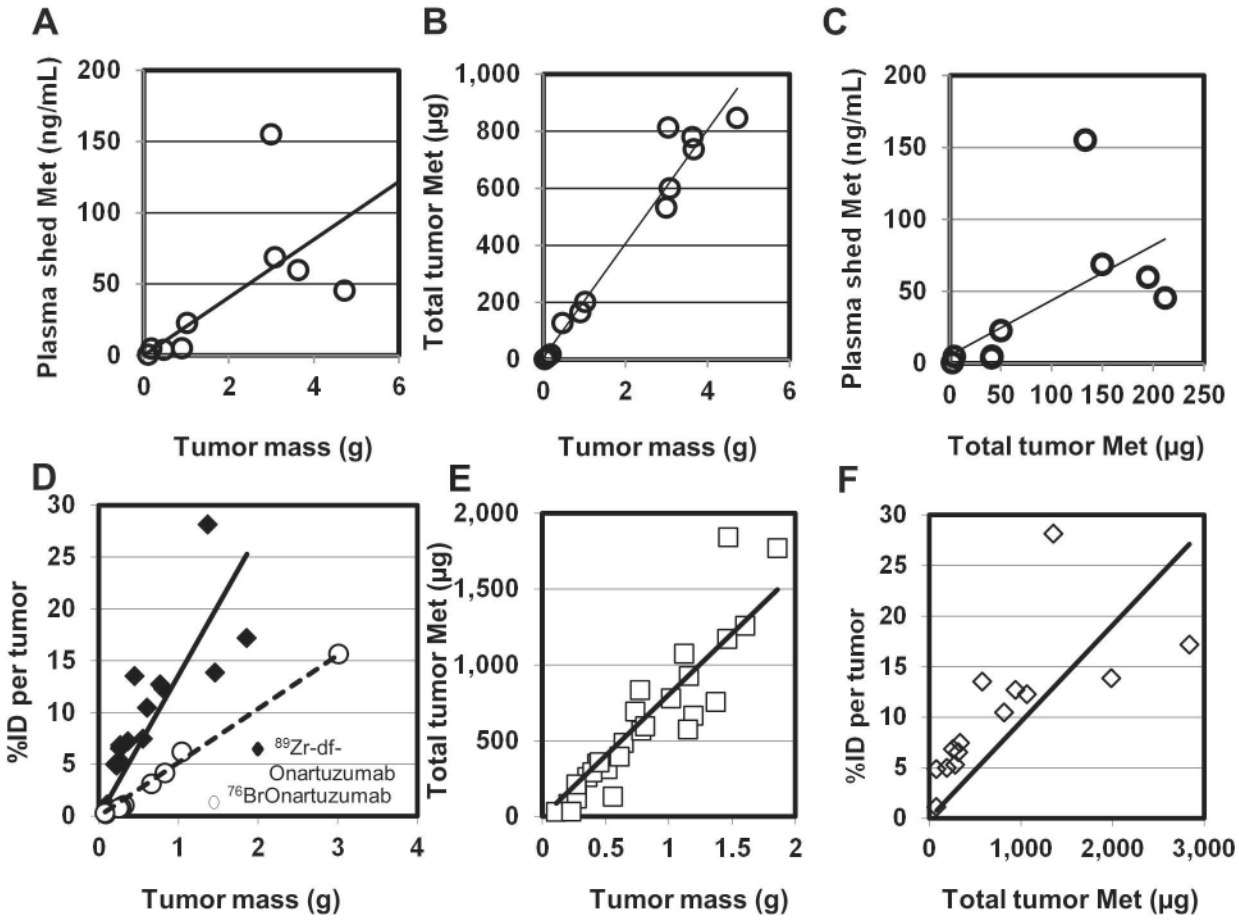

FIGURE 7.

Correlation of plasma shed Met, total Met tumor content, and radioactive tumor uptake (%ID per tumor) with tumor mass and Met abundance (all correlations determined using Spearman non-parametric analysis, r= Spearman r). **A-C)** Correlations of plasma and tumor samples from naïve MKN-45 xenografts: **A)** r = 0.8167; P< 0.02; **B)** r=0.9321; P<0.0001; **C)** r = 0.8167; P< 0.01. **D-F)** Tumor samples from MKN-45 xenografts previously injected with radiolabeled MetMAb: **D)** Correlations of radiolabeled Onartuzumab tumor uptake to tumor mass: ^{76}Br-Onartuzumab **(○)**: %ID per tumor determined after 24 h (r = 0.9879; P<0.0001); ^{89}Zr-df-Onartuzumab (◆): %ID per tumor determined after 3, 4, and 5 d(r = 0.9357; P<0.0001); **E)** Correlation of total tumor Met to mass: tumor samples were taken after 0.75, 1, 2, 3, 4 and 5 d of ^{89}Zr-df-Onartuzumab uptake and assayed for total Met content (r = 0.9721; P<0.0001); **F)** Correlation of ^{89}Zr-df-Onartuzumab tumor uptake (%ID per tumor after 3, 4, and 5 d of uptake) to total tumor Met determinations (r = 0.9385; P<0.0001).

TABLE 1

Comparison of tumor to muscle ratios of ^{89}Zr-df-Onartuzumab and ^{76}Br-Onartuzumab in MKN-45 xenografts from 6 h to 120 h.

	Tumor to muscle ratios*						
Time of Uptake (h)	**6**	**18**	**24**	**48**	**72**	**96**	**120**
^{89}Zr-df-Onartuzumab	--	**6.4** (0.4)	**7.1** (1.0)	**13.2** (2.4)	**12.2** (2.3)	**19.6** (2.4)	**26.6** (0.9)
^{76}Br-Onartuzumab	**3.7** (0.4)	**3.8** (0.4)	**4.5** (0.9)	**5.8** (0.7)	**5.3** (0.6)	--	--

*Each value represents the mean ratio with the standard deviation below in parenthesis; n= 5.